DOI: 10.61782/fa.2025.0571

FORUM ACUSTICUM EURONOISE 2025

MITIGATION STRATEGIES FOR ACOUSTIC REFLECTIONS GENERATED BY AN AXISYMMETRIC WIND TUNNEL NOZZLE

Luca Nicola Quaroni [1*] **Roberto Merino-Martínez** [1]

[1] Faculty of Aerospace Engineering, Delft University of Technology, the Netherlands

ABSTRACT

The issue of acoustic reflections caused by an axisymmetric nozzle is addressed both numerically and experimentally. The contraction (with an exit diameter of 420 mm and a contraction ratio of 2) is representative of typical open-jet wind tunnel exits. Such a category of wind tunnels are extensively used in aeroacoustic studies due to the possibility of acoustic treatment of the test chamber (plenum) walls and the placement of acoustic sensors outside of the flow. The distance between the wind tunnel's nozzle exit and the model being tested is usually limited to around one hydraulic diameter in order for the model to be fully contained within the exit jet's core. Partly for this reason, the wind tunnel nozzle normally protrudes inside the anechoic plenum to distance the tested model from the (acoustically-treated) walls. This effectively creates a cavity, which is in communication with the test section. Acoustic simulations through a commercial finite-element code (COMSOL Multiphysics) show that the presence of the nozzle leads to interference patterns within the test section and a substantial modification of a source's measured directivity pattern. Experimental measurements in a fully anechoic chamber confirm these results. Melamine foam inserts on both the exit flange and part of the inner walls of the contraction are shown to mitigate the issue partly.

Keywords: ***Acoustic reflections, Aeroacoustic wind tunnel, Melamine foam inserts.***

Corresponding author: *l.n.quaroni@tudelft.nl.*

1. INTRODUCTION

Awareness of the adverse health effects of noise exposure from the aviation sector has been steadily increasing over the past few decades as the volume of flights has increased globally [1]. Furthermore, in an effort to increase propulsive efficiency, novel architectures (i.e. distributed propellers, boundary layer ingestion, etc.) have been introduced, potentially contributing to and altering the noise generation [2]. Improvements in control technologies and the lowering of production costs have then led to the widespread use of small Unmanned Aerial Vehicles (UAVs) for both professional and entertainment purposes, further exacerbating the issue [3]. Research for mitigation strategies has therefore followed suit, with experimental testing usually involving anechoic chambers and/or open-jet wind tunnels. While offering anechoic conditions (i.e. free-field sound propagation) over a large frequency range, anechoic chambers lack the possibility of adding any inflow, restricting their use to hovering UAVs [4]. Open-jet wind tunnels, on the other hand, allow for the presence of low-turbulence subsonic inflows in an anechoic environment, making them the perfect candidates for aeroacoustic studies. Common designs present a turbulence-reducing contracting nozzle protruding into an anechoic plenum, matched by a collector on the opposite side for the creation of a semi-closed air circuit [5]. Recent contributions involving anechoic open-jet wind tunnels focused on isolated propellers [6, 7], propeller installation effects [8], and turbulence-airfoil interaction [9,10].

Because of the widespread use of open-jet anechoic wind tunnels in aeroacoustic investigations, a clear understanding of the effects related to their specific testing environment is essential for a correct interpretation of

the results obtained. The present paper focuses on the issue of acoustic reflections caused by an axisymmetric contracting nozzle designed for an open-jet wind tunnel facility. It summarizes the results of a numerical and experimental investigation of the acoustic interference patterns generated by a simple point sound source located outside of the nozzle's exit, representative of the typical location of test models. The effectiveness of acoustically absorbing panels at mitigating the issue is also discussed.

2. PROBLEM OVERVIEW

2.1 Contraction geometry

An axisymmetric contraction was designed as part of a broader investigation [7] of turbulence-ingestion noise generation by an isolated propeller at the anechoic wind tunnel facility (A-Tunnel) of Delft University of Technology [11]. The nozzle is intended to both improve the isotropy of grid-generated turbulence and reduce the grids' self-noise, following suggestions by Bowen et al. [12]. The contraction follows the fifth-order polynomial wall profile indicated by Bell & Mehta [13]:

$$\mathrm{D(z)} = \mathrm{D_{wt}} + (\mathrm{D_{wt}} - \mathrm{D_{ext}}) \left[-10 \left(\frac{z}{\mathrm{L_c}} \right)^3 + \right.$$
$$\left. + 15 \left(\frac{z}{\mathrm{L_c}} \right)^4 - 6 \left(\frac{z}{\mathrm{L_c}} \right)^5 \right], \quad (1)$$

where all the geometrical parameters and their values are shown in Fig. 1. The additional cylindrical section after the contracting profile, of length $\mathrm{L_a} = \mathrm{R_{wt}}/2 = 150$ mm, was inserted to improve the flow's homogeneity at the nozzle's exit. Two flanges with a thickness of 15 mm and six aluminum struts (see top view in Fig. 2) were included for both structural and practical reasons and for compatibility with existing nozzles designed for the same wind tunnel, e.g. [11, 14]. A hot-wire anemometry campaign showed that the contraction produces streamwise turbulence intensity levels u'/U_∞ lower than 0.1% with good flow homogeneity within the first diameter $\mathrm{D_{ext}}$ from the nozzle exit [7].

2.2 Example: interference patterns in turbulence-interaction noise investigation

Fig. 3 shows the experimental setup used for the aforementioned investigation of turbulence-interaction noise by

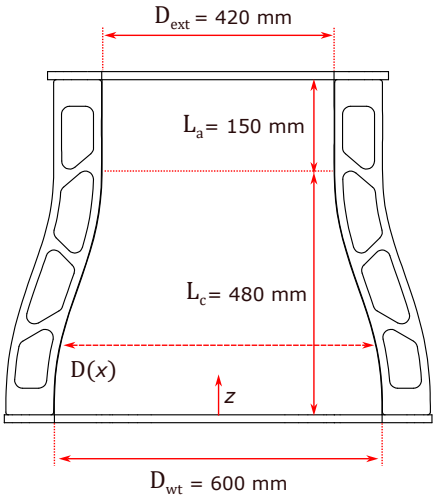

Figure 1. Sectional view of the axisymmetric contraction. The flow is in the positive z direction.

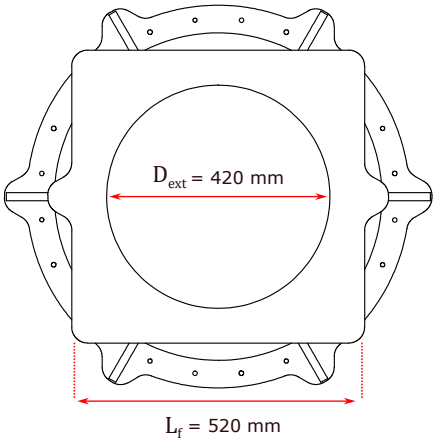

Figure 2. Top view of the axisymmetric contraction.

an isolated propeller. A turbulence-generating grid was inserted between the main wind tunnel's exit on the floor and the inlet of the additional contraction, allowing for the generation of turbulence intensity levels in the streamwise direction z of approximately 3% at the location of the propeller's disk ($z = 0.4\,\mathrm{D_{ext}}$, with $z = 0$ m at the nozzle exit plane). For further details, the reader is referred to Quaroni et al. [7]. The self-noise produced by the supporting structure and the propeller's nacelle was obtained by substituting the propeller with a dummy spinner and installing or removing the turbulence-producing grid at the base of the additional contraction. The self-noise of the system

composed of the nozzle and grid only was also tested by removing the propeller's setup altogether.

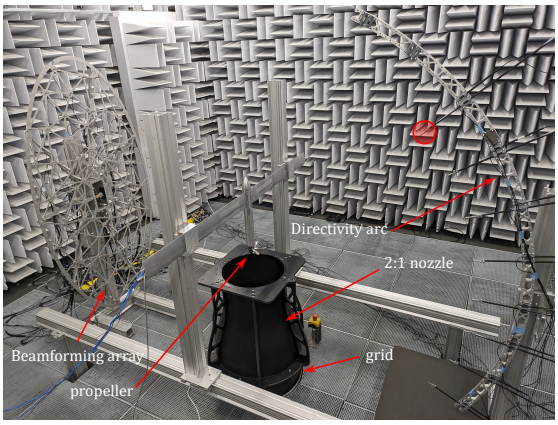

Figure 3. Overview of the setup for the study of turbulence-interaction noise by an isolated propeller, from [7]. Microphone at $\vartheta = 50°$ highlighted.

Fig. 4 reports the power spectral density (PSD) of the acoustic pressures measured at a distance $r = 1.3$ m from the center of the propeller's disk and at emission angle $\theta = 50°$ downstream of the propeller's disk for the self-noise cases and the condition with an operational propeller spinning at 180.57 Hz; a common inflow velocity of $V_\infty = 30$ m/s was set. Characteristic undulations in the broadband spectra are clearly visible in all cases. Oscillation 'amplitudes' increase while their 'wavelengths' remain constant when going from the case of clean inflow to the support structure to the case of turbulent inflow and installed propeller. This observation seems to indicate that the behavior might be related to the acoustic response of the overall wind tunnel system rather than to a particular sound generation mechanism (e.g. turbulence-ingestion noise). For the cases of 'grid on' and 'propeller setup on-off', the spectral oscillations almost perfectly overlap for frequencies higher than $\approx$ 2000 Hz, indicating that the acoustic scattering due to the support structure has a limited effect. Finally, a previous characterization of the wind tunnel facility showed that the anechoic plenum has a cut-off frequency of 200 Hz [11]. This leads to the conclusion that the newly designed axisymmetric nozzle might be responsible for the introduction of spurious acoustic reflections, leading to complex interference patterns within the anechoic plenum of the wind tunnel. The following sections explore this possibility through a numerical and experimental investigation of the acoustic properties of the contraction.

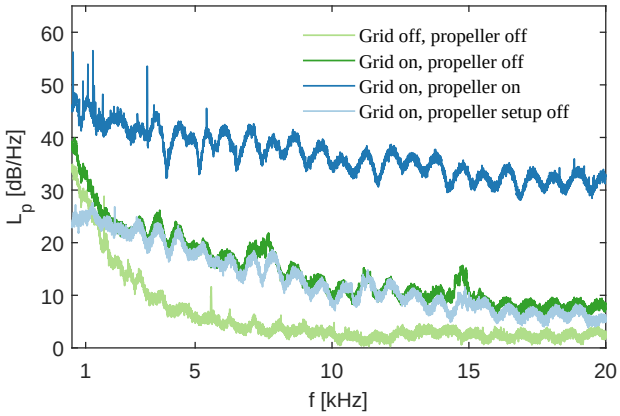

Figure 4. Power spectral density (L_p, $\Delta f = 1$ Hz) of acoustic pressure at $r = 1.3$ m and $\theta = 50°$ downstream of propeller's disk for the case of: no grid and dummy spinner, grid and dummy spinner, grid and propeller, grid on and propeller setup off ($V_\infty = 30$ m/s).

3. NUMERICAL INVESTIGATION

The commercial software COMSOL Multiphysics 6.2 was used to gain insight into the acoustic scattering effects caused by the introduction of the axisymmetric nozzle to the wind tunnel's anechoic plenum.

3.1 Numerical model

A simplified geometry of the nozzle was considered in order to reduce the problem to a 2D axisymmetric one. Both the bottom flange and the side struts were removed, while the shape of the top flange was converted from a square with rounded edges to an infinitely thin circular plate. This allowed for a considerable reduction in computational costs while maintaining the main parameters of interest to the problem. Fig 5 reports a sketch of the numerical domain. An acoustic point source of strength Q_s was placed at $z_s = \mathrm{L}_c + \mathrm{h}_s$, with $\mathrm{h}_s = 0.4\,\mathrm{D}_{\mathrm{ext}} = 164$ mm being the distance of the source from the nozzle exit (same as the distance to the propeller disk in the example before). The value of Q_s was computed from the formula for monopole sources [15]:

$$p_{rms}^2 = \frac{Q_s^2 k^2 (\rho_0 c^2)}{16\pi^2 r^2 (1 + k^2 a^2)} \tag{2}$$

where $k = 2\pi f_s/c = \omega_s/c$ is the wave number and a is the source radius. Letting $a \to 0$ and imposing p_{rms} such that the sound pressure level $L_p = 45$ dB/Hz at a distance $r = 1.3$ m, a value of for Q_s could be computed for each simulated source frequency f_s. Such distance was set equal to the inner radius of the directivity arc shown in Fig. 4 (and used in the experimental analysis discussed in Section 4).

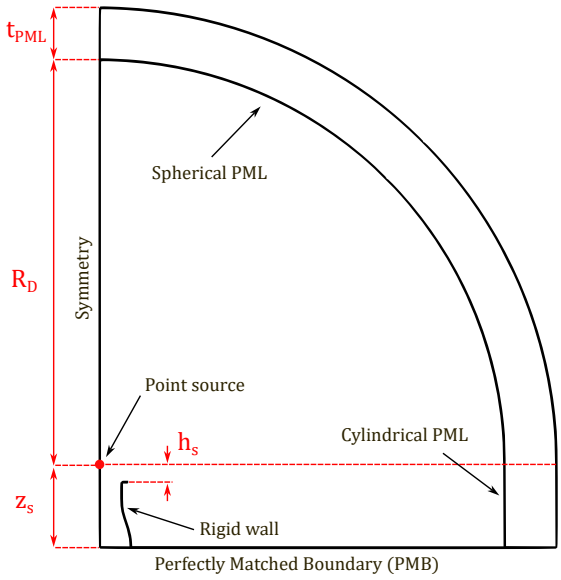

Figure 5. Sketch of the numerical domain including source position and boundary conditions.

To reproduce acoustic free-field propagation conditions, Perfectly Matched Layers (PML) and a Perfectly Matched Boundary (PMB) were added to the numerical domain's boundaries. A spherical and a cylindrical PML enclosed the top and right boundaries while a PMB represents the floor of the anechoic chamber. At least 5 cells per acoustic wavelength λ are recommended for a correct discretization of an acoustic field [16]. In the present case, the maximum cell size in the domain was set to $h_{max} = \lambda/8$. Preliminary simulations without the inclusion of the rigid-walled contraction showed that free-field conditions were obtained when imposing a radius of the numerical domain $\mathrm{R}_D = 4$ m $\approx 20\mathrm{D}_{ext}$ and a PML thickness $t_{PML} = 0.5$ m. This last value is related to the ability of the PML to absorb incoming waves and should be in the order of the largest wavelength to absorb. The application of acoustically absorbing panels to mitigate the interference caused by the nozzle was also numerically explored. Melamine foam was selected over other materials (e.g. glass wool, polyurethane foam) due to its better acoustic performance when grazing flows are involved [17]. Foam inserts were applied on both the upper flange and on the internal walls of the end (cylindrical) section of the nozzle (Fig. 6). This was done to minimize the possible influence of the foam layers on the flow quality (homogeneity and turbulence intensity) of the nozzle. The Johnson-Champoux-Allard (JCA) model was used to model the acoustic absorption by the melamine foam inserts, with the required physical properties listed in Table 1.

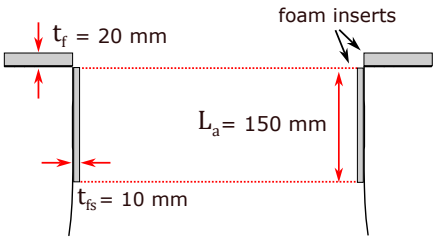

Figure 6. Diagram of melamine foam inserts on the upper end of the simplified contraction geometry.

Table 1. Melamine foam properties, from [18].

Quantity	Symbol	Value
Porosity	ε_p	0.95
Flow resistivity	R_f	10500 Pa · s/m^2
Drained density	ρ_d	11 kg/m^3
Viscous length (coeff.)	s	0.49
Thermal length	L_{th}	470 μm

3.2 Results

The sound pressure level distribution over the numerical domain for the untreated contraction and a source frequency $f_s = 4000$ Hz is reported in Fig. 7. Such frequency corresponds to a Helmholtz number $He = 2\pi L/\lambda \approx 31$, where $L = D_{ext}$, which is within the typical frequency range of interest for aeroacoustic testing. A complex pattern of alternating lobes is present due to constructive and destructive interference. This clearly shows the deviation in terms of directivity with respect to the

spherical propagation expected for a point sound source and typically assumed in acoustic beamforming [11].

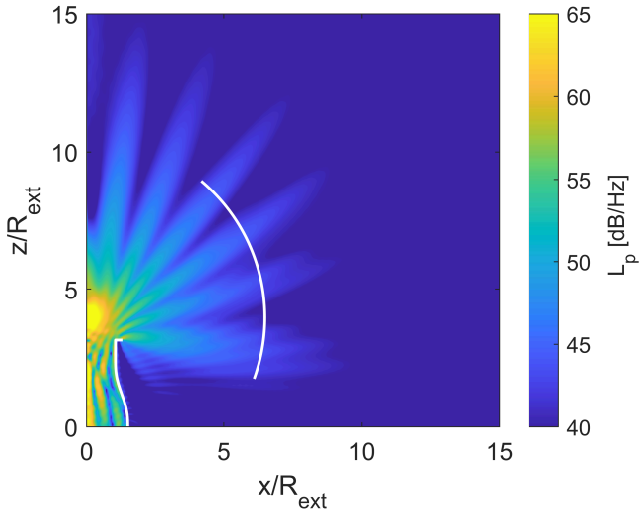

Figure 7. Simulated sound pressure level (L_p) distribution for the case of the untreated (simplified) nozzle geometry and an acoustic point source with frequency $f_s = 4000$ Hz at a distance $h_s = 0.4\mathrm{D}_{ext}$ from the nozzle exit. The directivity arc and nozzle outline are highlighted in white.

Figs. 8-10 depict the directivity patterns of L_p at $r = 1.3$ m and polar angles $\vartheta = [-20°, 50°]$ (with $\vartheta = 0°$ corresponding to the nozzle exit plane and ϑ positive anti-clockwise) for three different source frequencies $f_s = 1000$ Hz, 4000 Hz and 6300 Hz. Both cases of untreated and acoustically treated nozzle are reported. The range for ϑ is chosen to be consistent with the angle covered by the directivity arc shown in Fig. 3 and used in the experimental investigation (Sec. 4). The source frequencies f_s correspond to a selection of typical 1/12-octave band center frequencies of interest during aeroacoustic investigations. Large differences in L_p along the arc length are visible at all source frequencies, with the number of lobes increasing with increasing f_s. The addition of melamine foam helps to some extent in reducing the amplitude of the lobes and its effectiveness increases with increasing f_s. This last consideration had to be expected since the foam inserts' small thickness limits the dampening of longer wavelengths (i.e. lower frequencies).

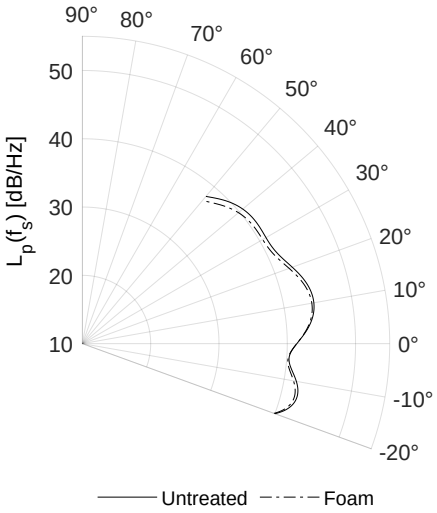

Figure 8. Simulated sound pressure level L_p directivity at $r = 1.3$ m ($r/R_{ext} \approx 6$) for a single source frequency of $f_s = 1000$ Hz.

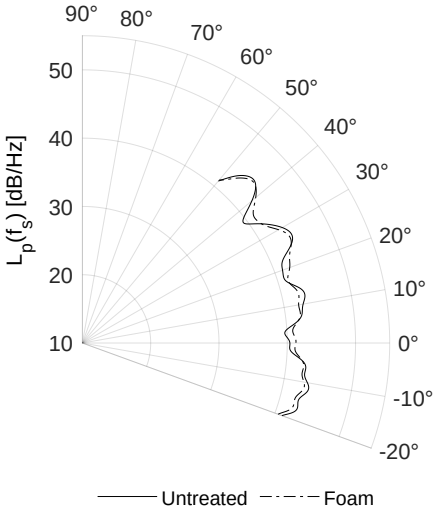

Figure 9. Simulated sound pressure level L_p directivity at $r = 1.3$ m ($r/R_{ext} \approx 6$) for a single source frequency of $f_s = 4000$ Hz.

4. EXPERIMENTAL INVESTIGATION

An experimental campaign was conducted to confirm the effectiveness of the melamine foam treatment in mitigating the issue of acoustic reflections by the presence of the nozzle.

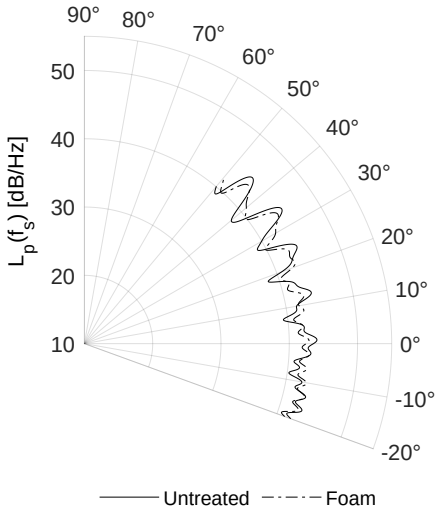

Figure 10. Simulated sound pressure level L_p directivity at $r = 1.3$ m ($r/R_{ext} \approx 6$) for a single source frequency of $f_s = 6300$ Hz.

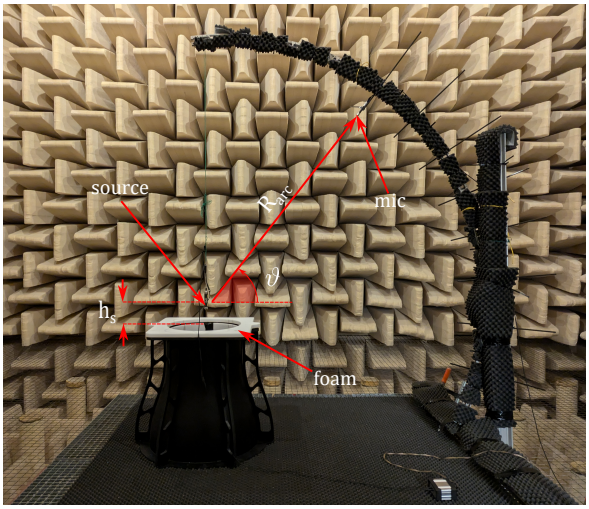

Figure 11. Experimental setup at the anechoic chamber of Delft University of Technology.

4.1 Experimental setup

The experiment was conducted at the 8 m × 8 m × 8 m anechoic chamber of the Applied Sciences faculty of Delft University of Technology (Fig. 11). A miniature sound source (Qsources, type QindW) was positioned at a distance $h_s = 0.4\mathrm{D_{ext}}$ above the center of the contraction's exit ($r = 0$). The source presents good omnidirectionality properties over the frequency range from 500 Hz to 7000 Hz and an accompanying amplifier allows for the production of white noise in this range [19]. The same directivity arc shown in Fig. 3 was employed to sample the acoustic pressure field at a distance $r = R_{arc} = 1.3$ m over the polar angle range $\vartheta = [-20°, +50°]$ with a step $\Delta\vartheta = 10°$. A prepolarized 1/2-inch free-field microphone (Brüel & Kjær, Type 4189) was sequentially moved along the directivity arc and its signal was acquired for 45 s and sampled at 40 kHz through a hand-held analyzer (Brüel & Kjær, Type 2250).

4.2 Results

Figure 12 presents the power spectral density at $\vartheta = 50°$ for the untreated and the acoustically treated nozzle. Oscillations in the spectra are visible in both cases. However, the addition of the melamine foam layer effectively reduces their amplitude over the considered frequency range. Figs. 13-15 report the 1/12-octave band sound pressure level $L_{p_{1/12}}$ directivity plots for the center frequencies of $f_c = 1000$ Hz, 4000 Hz, and 6300 Hz. The $L_{p_{1/12}}$ is computed as:

$$L_{p_{1/12}}(f_c) = 10\log_{10}\left(\sum_{n=1}^{N}\frac{S_{pp}(f_i)\Delta f}{p_{ref}^2}\right), \qquad (3)$$

where $f_1 = f_L$ and $f_N = f_U$ are the lower and upper bounds of the 1/12-octave band with center frequency f_c, S_{pp} is the acoustic power spectral density, Δf is its frequency interval, and $p_{ref} = 20$ μPa is the reference acoustic pressure. At the lowest frequency, the pattern is highly non-omnidirectional but foam addition seems to nonetheless mitigate the issue by reducing the $L_{p_{1/12}}$ difference between points along the arc. For the larger center frequencies, the increase in frequency bandwidth considered in the computation of the $L_{p_{1/12}}$ makes the overall directivity closer to the omnidirectional one. However, it is also evident that adding foam has the effect of improving the source omni-directionality, especially at larger polar angles ϑ.

5. CONCLUSIONS

The present paper has dealt with the issue of acoustic interference by an axisymmetric contraction in an open-jet wind tunnel exit. It was shown through both numerical

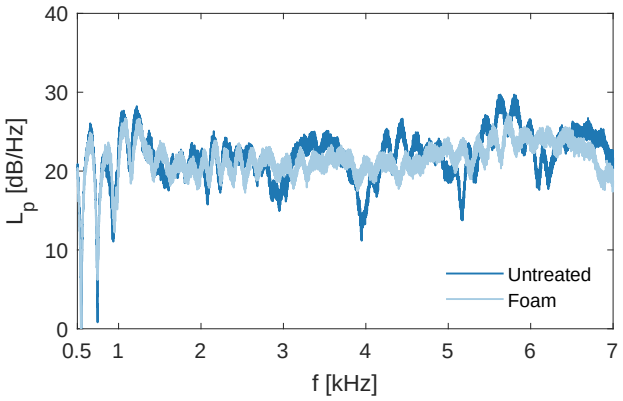

Figure 12. Power spectral density of microphone signal at $\vartheta = 50°$ for both acoustically treated and untreated nozzle ($\Delta f = 1$ Hz).

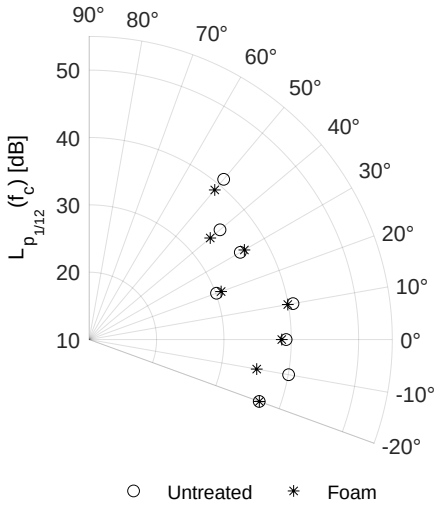

Figure 13. Directivity of 1/12-octave band sound pressure level $L_{p_{1/12}}$ at center frequency $f_c = 1000$ Hz and $r = 1.3$ m ($r/R_{ext} \approx 6$) for both acoustically treated and untreated nozzle.

and experimental analyses that the introduction of the nozzle to an anechoic environment caused substantial modifications in the directivity pattern of a simple point source placed at a typical position of aeroacoustic sources in wind tunnel testing. Adding melamine foam inserts on the upper flange and along the end section of the internal wall of the contraction helped mitigate the issue to some extent.

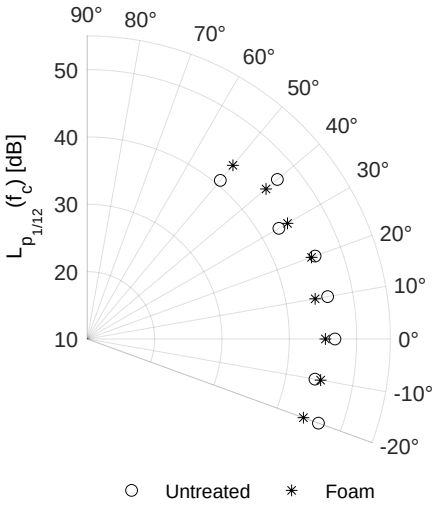

Figure 14. Directivity of 1/12-octave band sound pressure level $L_{p_{1/12}}$ at center frequency $f_c = 4000$ Hz and $r = 1.3$ m ($r/R_{ext} \approx 6$) for both acoustically treated and untreated nozzle.

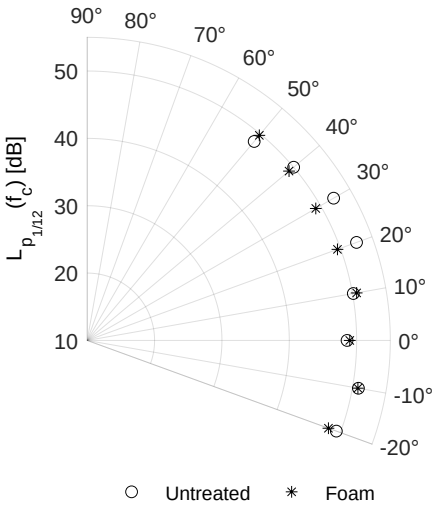

Figure 15. Directivity of 1/12-octave band sound pressure level $L_{p_{1/12}}$ at center frequency $f_c = 6300$ Hz and $r = 1.3$ m ($r/R_{ext} \approx 6$) for both acoustically treated and untreated nozzle.

6. ACKNOWLEDGMENTS

This work is part of the HOPE (Hydrogen Optimized multi-fuel Propulsion system for clean and silEnt air-

craft) project and has received funding from the European Union's Horizon Europe research and innovation programme under grant agreement No. 101096275. The authors would also like to acknowledge the help of Bieke von den Hoff during the experimental campaign in the anechoic chamber, as well as the support from Henry den Bok from the faculty of Applied Sciences.

7. REFERENCES

[1] L. Leylekian, A. Covrig, and A. Maximova, eds., *Aviation Noise Impact Management: Technologies, Regulations, and Societal Well-being in Europe*. Cham: Springer International Publishing, 2022.

[2] N. van Arnhem, *Unconventional PropellerAirframe Integration for Transport Aircraft Configurations*. PhD thesis, Delft University of Technology, 2022.

[3] N. Green, A. J. Torija, and C. Ramos-Romero, "Perception of noise from unmanned aircraft systems: Efficacy of metrics for indoor and outdoor listener positions," *The Journal of the Acoustical Society of America*, vol. 155, pp. 915–929, Feb. 2024.

[4] C. E. Tinney and J. Sirohi, "Multirotor Drone Noise at Static Thrust," *AIAA Journal*, vol. 56, pp. 2816–2826, July 2018.

[5] C. S. Allen, W. K. Blake, R. P. Dougherty, D. Lynch, P. T. Soderman, and J. R. Underbrink, *Aeroacoustic Measurements*. Berlin, Heidelberg: Springer Berlin Heidelberg, 2002.

[6] K. Baskaran, N. S. Jamaluddin, A. Celik, D. Rezgui, and M. Azarpeyvand, "Effects of number of blades on propeller noise," *Journal of Sound and Vibration*, vol. 572, p. 118176, Mar. 2024.

[7] L. N. Quaroni, R. Merino-Martinez, F. D. Monteiro, and S. S. Kumar, "Collective blade pitch angle effect on grid turbulence ingestion noise by an isolated propeller," in *30th AIAA/CEAS Aeroacoustics Conference (2024)*, (Rome, Italy), American Institute of Aeronautics and Astronautics, June 2024.

[8] F. Petricelli, P. Chaitanya, S. Palleja-Cabre, S. Meloni, P. F. Joseph, A. Karimian, S. Palani, and R. Camussi, "An experimental investigation on the effect of in-flow distortions of propeller noise," *Applied Acoustics*, vol. 214, p. 109682, Nov. 2023.

[9] T. Geyer, S. Wasala, and E. Sarradj, "Experimental Study of Airfoil Leading Edge Combs for Turbulence Interaction Noise Reduction," *Acoustics*, vol. 2, pp. 207–223, Apr. 2020.

[10] L. Bowen, A. Celik, and M. Azarpeyvand, "A thorough experimental investigation on airfoil turbulence interaction noise," *Physics of Fluids*, vol. 35, p. 035123, Mar. 2023.

[11] R. Merino-Martínez, A. Rubio Carpio, L. T. Lima Pereira, S. Van Herk, F. Avallone, D. Ragni, and M. Kotsonis, "Aeroacoustic design and characterization of the 3D-printed, open-jet, anechoic wind tunnel of Delft University of Technology," *Applied Acoustics*, vol. 170, p. 107504, Dec. 2020.

[12] L. Bowen, A. Celik, M. Azarpeyvand, and C. R. I. Da Silva, "Grid Generated Turbulence for Aeroacoustic Facility," *AIAA Journal*, vol. 60, pp. 1833–1847, Mar. 2022.

[13] J. Bell and R. Mehta, "Contraction Design for Small Low-Speed Wind Tunnels," Contractor report 177488, NASA, 1988.

[14] E. Grande, G. Romani, D. Ragni, F. Avallone, and D. Casalino, "Aeroacoustic Investigation of a Propeller Operating at Low Reynolds Numbers," *AIAA Journal*, vol. 60, pp. 860–871, Feb. 2022.

[15] M. Norton and D. Karczub, "2 Sound waves: a review of some fundamentals," in *Fundamentals of Noise and Vibration Analysis for Engineers*, Cambridge University Press, 2nd ed., 2003.

[16] COMSOL, "Acoustics Module: User's Guide," 2018.

[17] H. F. Bento, D. Ragni, F. Avallone, D. Simons, and M. Snellen, "Acoustic wall treatments for wind tunnel aeroacoustic measurements," *Applied Acoustics*, vol. 199, p. 108989, Oct. 2022.

[18] N. Kino and T. Ueno, "Comparisons between characteristic lengths and fibre equivalent diameters in glass fibre and melamine foam materials of similar flow resistivity," *Applied Acoustics*, vol. 69, pp. 325–331, Apr. 2008.

[19] H. F. Mourão Bento, C. P. VanDercreek, F. Avallone, D. Ragni, P. Sijtsma, and M. Snellen, "Wave propagation modelling approach for improved assessment of the acoustic field in closed test section wind tunnels," *Journal of Sound and Vibration*, vol. 600, p. 118858, Mar. 2025.